Research Article Vol. 36, No. 2 / February 2019 / Journal of the Optical Society of America B 493

Journal of the Optical Society of America B

OPTICAL PHYSICS

Ultrafast time-domain wave packet evolution of atomic photoionization

Rui-Hua Xu,[1] Zhaoyan Zhou,[2] and Xu Wang[1,*]

[1]Graduate School, China Academy of Engineering Physics, Beijing 100193, China
[2]Department of Physics, National University of Defense Technology, Changsha 410073, China
*Corresponding author: xwang@gscaep.ac.cn

Received 12 September 2018; revised 6 January 2019; accepted 6 January 2019; posted 7 January 2019 (Doc. ID 345520); published 31 January 2019

We present a combined numerical and theoretical study of atomic photoionization in the time domain. We show how a photoelectron wave packet rapidly changes its shape after being emitted, from a complex multipeak structure to eventually a relatively simple single-peak structure. This time-domain shape evolution provides information beyond the time-dependent average position of the wave packet, which for example has been used to retrieve the Wigner time delay. For few-cycle laser pulses, the asymptotic velocity of the photoelectron can be different from long-pulse-based expectations due to non-negligible changes of the dipole matrix element within the spectra of the laser pulses.

https://doi.org/10.1364/JOSAB.36.000493

1. INTRODUCTION

The photoelectric effect known today can be traced back to the experiments by Hertz [1] and by Lenard [2] in the late 19th and the early 20th centuries. These experiments had motivated Einstein's quanta theory of light [3]. Existing in any material, the photoelectric effect has been extensively studied also in the context of atomic photoionization [4–14], especially with the advent of synchrotron radiations, which allow the generation of high-energy photons with tunable frequencies.

Virtually all studies on atomic photoionization, and on the photoelectric effect in general, focused on the energy or the momentum domain. With rapid advancements of ultrafast laser technologies, however, light pulses with femtosecond or subfemtosecond durations can be routinely generated. Table-top titanium:sapphire lasers can generate near-infrared pulses of femtosecond durations. Free electron lasers can generate femtosecond pulses in the x-ray regime. Based on high harmonic generation, isolated light pulses of durations of a few tens of attoseconds have been reported [15–17]. Hard x-ray pulses of 200 attoseconds' duration have also been reported using free-electron lasers at the Linac Coherent Light Source [18]. These ultrashort light sources have enabled investigations of ultrafast dynamical processes in the time domain, such as following electron localization in molecules [19], real-time observation of Auger decay [20], real-time observation of electron tunneling ionization [21], charge transfer in polyatomic molecules [22,23], real-time buildup of Fano resonances [24], attosecond time delays in atomic photoionization [25–35], etc.

The availability of these ultrashort light sources motivates us to (re)think about the photoionization process from the time-domain perspective. How exactly does photoionization happen? What is the shape of the photoelectron wave packet after being emitted? How does it evolve with time? These are the questions that we are interested in and are to be answered in the current paper. Somehow surprisingly, these questions have not been answered in the literature, as far as we are aware of.

By numerically solving a time-dependent Schrödinger equation (TDSE) in full dimensions, we show how the photoelectron wave packet is created and evolves with time. We find that the wave packet has a rather complex multipeak structure right after being emitted, but it rapidly adjusts its shape, reduces the number of peaks, and eventually evolves into a relatively simple single-peak structure. These numerical results can be qualitatively understood from the time-dependent perturbation theory. The shape evolution will be explained through the temporal evolution of the phase of the photoelectron wave packet.

We will also show that for few-cycle laser pulses, the asymptotic velocity of the photoelectron can be different from normal, long-pulse-based expectations. For short laser pulses with relatively broad spectra, the dipole transition matrix element may change appreciably within the spectra of the laser pulses, shifting the average momentum and the asymptotic velocity of the photoelectron wave packet. Depending on the detailed form of the dipole transition matrix element, the photoelectron wave packet may be faster or slower than that generated with long pulses.

This paper is organized as follows. In Section 2 we introduce the methods that we use, including a numerical method for solving the TDSE and the time-dependent perturbation theory for interpretation of numerical results. In Section 3 we present

our numerical results and the corresponding analyses and discussions. A conclusion is given in Section 4.

2. METHODS

A. Numerical Solution of the TDSE

The TDSE for atomic hydrogen interacting with an external laser field can be written as (in atomic units)

$$i\frac{\partial}{\partial t}\psi(\mathbf{r},t)=\hat{H}\psi(\mathbf{r},t)=[\hat{H}_0+\hat{H}_I]\psi(\mathbf{r},t), \tag{1}$$

where $\hat{H}_0$ is the field-free Hamiltonian and $\hat{H}_I$ is the atom-field interaction

$$\hat{H}_0=-\frac{1}{2}\frac{d^2}{dr^2}+\frac{\hat{L}^2}{2r^2}+V(r), \tag{2}$$

$$\hat{H}_I=\mathbf{r}\cdot\hat{\mathbf{e}}_z\varepsilon(t)=\varepsilon(t)r\cos\theta. \tag{3}$$

For the hydrogen atom, $V(r)=-1/r$, and we have used the length-gauge form of the interaction Hamiltonian. The laser field $\varepsilon(t)=\varepsilon_0 f(t)\cos\omega t$ is assumed to be linearly polarized along the z direction with amplitude ε_0 and angular frequency ω. A trapezoidal pulse envelope function $f(t)$ has been used; it has a two-cycle turning on and a two-cycle turning off,

$$f(t)=\begin{cases} t/2T & 0<t\le 2T \\ 1 & 2T<t\le \tau-2T \\ (-t+\tau)/2T & \tau-2T<t\le\tau \end{cases}, \tag{4}$$

where $T=2\pi/\omega$ is the duration of an optical cycle and τ is the duration of the whole pulse.

We use a generalized pseudospectral method [36] to numerically solve the TDSE. The Schrödinger equation can be propagated in discrete time steps as

$$\begin{aligned}\psi(\mathbf{r},t+\Delta t)\simeq&\exp(-i\hat{H}_0\Delta t/2)\\&\times\exp[-i\hat{H}_I(r,\theta,t+\Delta t)\Delta t]\\&\times\exp(-i\hat{H}_0\Delta t/2)\psi(\mathbf{r},t)+O(\Delta t^3).\end{aligned} \tag{5}$$

The time propagation of the wave function from t to $t+\Delta t$ is achieved by three steps: (i) propagation for half a time step $\Delta t/2$ in the energy space spanned by $\hat{H}_0$; (ii) transformation to the coordinate space and propagation for one time step Δt under the atom-field interaction $\hat{H}_I$; and (iii) transformation back to the energy space spanned by $\hat{H}_0$ and propagation for another half time step $\Delta t/2$. The commutation errors are on the order of Δt^3.

The wave function $\psi(\mathbf{r},t)$ can be expanded in Legendre polynomials

$$\psi(r_i,\theta_j,t)=\sum_{l=0}^{l\,\max}g_l(r_i)P_l(\cos\theta_j), \tag{6}$$

if the atom is initially in an s state (the magnetic quantum number $m=0$), and the laser polarization is linear ($\Delta m=0$). The $g_l(r_i)$ is calculated by the Gauss–Legendre quadrature

$$g_l(r_i)=\sum_{k=1}^{L+1}w_k P_l(\cos\theta_k)\psi(r_i,\theta_k,t), \tag{7}$$

where quadrature lattices $\cos\theta_k$ are zeros of the Legendre polynomials $P_{L+1}(\cos\theta_k)$ and w_k is the corresponding quadrature weights.

Now the evolution of the wave function in the energy space spanned by $\hat{H}_0$ can be written as

$$\begin{aligned}&\exp(-i\hat{H}_0\Delta t/2)\psi(r_i,\theta_j,t)\\&=\sum_{l=0}^{l\,\max}[\exp(-i\hat{H}_0^l\Delta t/2)g_l(r_i,t)]P_l(\cos\theta_j).\end{aligned} \tag{8}$$

Each g_l is propagated independently within individual $\hat{H}_0^l$ energy space.

To avoid artificial boundary reflection, for each time step a mask function $M(r)=\cos^{1/4}[\frac{\pi}{2}(r-r_0)/(r_m-r_0)]$ is multiplied to the wave function for $r\ge r_0$. Here r_0 is the entrance radius of the absorbing region and r_m is the radius of the numerical grid.

B. Time-Dependent Perturbation Theory

From the time-dependent perturbation theory [37], the transition amplitude from an initial (bound) state $\psi_0(\mathbf{r})$ to a final continuum state $\psi_k(\mathbf{r})$ is

$$\begin{aligned}c(k,t)&=-i\int_0^t dt'\langle\psi_k(\mathbf{r})|\hat{H}_I(t)|\psi_0(\mathbf{r})\rangle e^{i\omega_0 t'}\\&=-i\varepsilon_0 D(k)\int_0^t dt'\cos\omega t' e^{i\omega_0 t'},\end{aligned} \tag{9}$$

where $D(k)\equiv\langle\psi_k(\mathbf{r})|r\cos\theta|\psi_0(\mathbf{r})\rangle$ is the dipole transition matrix element and ω_0 is the energy difference between the two states; for the purpose of analytical simplicity we have assumed $f(t)=1$. $\psi_0(\mathbf{r})$ and $\psi_k(\mathbf{r})$ are eigenstates of the unperturbed Hamiltonian $\hat{H}_0$, and they can be obtained numerically by solving the corresponding eigenvalue problem. We can proceed

$$\begin{aligned}c(k,t)&=-i\frac{\varepsilon_0 D(k)}{2}\int_0^t dt'[e^{i(\omega_0+\omega)t'}+e^{i(\omega_0-\omega)t'}]\\&=-\frac{\varepsilon_0 D(k)}{2}\left[\frac{e^{i(\omega_0+\omega)t}-1}{\omega_0+\omega}+\frac{e^{i(\omega_0-\omega)t}-1}{\omega_0-\omega}\right].\end{aligned} \tag{10}$$

For laser frequencies not far away from resonance, i.e., $|\omega_0-\omega|\ll\omega_0+\omega$, we can apply the rotating wave approximation by neglecting the first term in the square bracket

$$\begin{aligned}c(k,t)&\approx-\frac{\varepsilon_0 D(k)}{2}\frac{e^{i(\omega_0-\omega)t}-1}{\omega_0-\omega}\\&=-i\varepsilon_0 D(k)\frac{\sin[(\omega_0-\omega)t/2]}{\omega_0-\omega}e^{i(\omega_0-\omega)t/2}.\end{aligned} \tag{11}$$

In the above formula, $\omega_0=\omega_0(k)=I_p+k^2/2$ (for weak laser fields where ponderomotive shifts can be neglected), as illustrated schematically in Fig. 1.

The ionized wave packet for a particular partial wave in the configuration space is given by the radial wave function

$$R_l(r,t)=\int_0^\infty dk\, c(k,t)R_{kl}(r)e^{-ik^2t/2}. \tag{12}$$

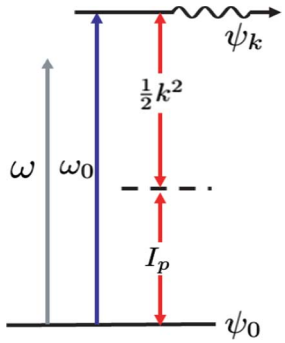

Fig. 1. Schematic illustration of the energies (frequencies) involved in atomic photoionization. The laser frequency is ω, which induces a transition from a bound state ψ_0 to a possible continuum state ψ_k. The energy difference between the two states is ω_0, which may not be in exact resonance to ω. ω_0 can be approximately divided into the ionization potential I_p and the kinetic energy of the emitted electron $k^2/2$, if the ponderomotive shifts can be neglected.

3. RESULTS AND DISCUSSION

A. Shape Evolution of the Photoelectron Wave Packet

Figure 2 shows time-domain shape evolutions of photoelectron wave packets, for three different laser pulse durations, namely, 3 fs (left column), 9 fs (middle column), and 15 fs (right column). The laser intensity 10^{13} W/cm^2 and the laser frequency is $\omega = 1.0$ a.u.. For exact resonance where $\omega_0 = \omega$, the wave number is denoted as k_0, which satisfies

$$\frac{k_0^2}{2} = \omega - I_p = 0.5 \text{ a.u.}, \quad \text{or} \quad k_0 = 1 \text{ a.u.} \tag{13}$$

For each panel, the horizontal axis is the distance (in atomic units) from the remaining ion, and the vertical axis is the radial wave packet $r^2|R(r)|^2$. Since we start from the ground state of the hydrogen atom, and the laser field is linearly polarized, only one partial wave ($l = 1$, $m = 0$) is involved in the continuum states.

We see from all the three examples that right after, or shortly after the laser pulse is over (e.g., the top two rows), the photoelectron wave packet has a rather complex multipeak structure. As time evolves, the wave packet quickly adjusts its shape (while at the same time translating in space), and the number of peaks reduces. Eventually a relatively simple single-peak structure emerges. The time scale of this shape evolution process depends on the duration of the laser pulse. For the three pulse durations that we use in Fig. 2, this shape adjusting process lasts for a few tens of femtoseconds to a few hundred femtoseconds. The wave packet will keep spreading in later times (not shown), maintaining a single-peak structure.

This shape evolution of the photoelectron wave packet provides richer information beyond the average position $\langle r \rangle(t)$,

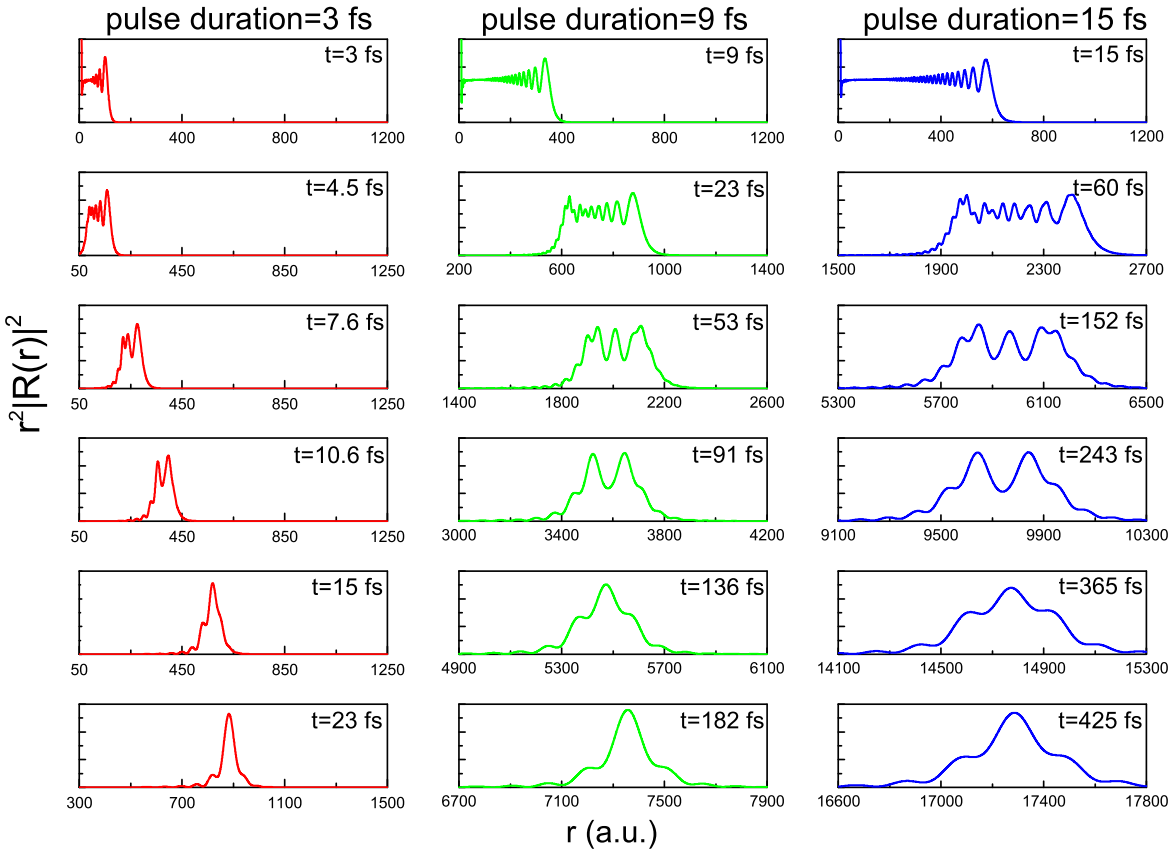

Fig. 2. Time evolution of the shape of the emitted photoelectron wave packet for three different laser pulse durations, namely, 3 fs (left column), 9 fs (middle column), and 15 fs (right column). The time for each snapshot is given in the upper right corner of each panel. For all three cases, the laser frequency $\omega = 1.0$ a.u., corresponding to 0.15 fs per optical cycle, and the laser peak intensity is 10^{13} W/cm^2.

extrapolation of which backward in time yields the Wigner time delay [26,38,39]. It remains open the possibility of utilizing the detailed shape information (e.g., $\langle r^2\rangle(t)$, $\langle r^3\rangle(t)$, etc.) to facilitate understandings about the photoionization process.

B. Qualitative Understandings from the Time-Dependent Perturbation Theory

The shape evolutions of the photoelectron wave packets given in Fig. 2 are obtained numerically by solving the full dimensional TDSE. In this subsection we give a qualitative understanding of the main features using the time-dependent perturbation theory.

For simplicity we consider in one dimension and assume that the continuum states are plane waves $\psi_k(x) = e^{ikx}$. From Eqs. (11) and (12) the wave packet in the configuration space is

$$\psi(x,t) = -i\varepsilon_0 \int_0^\infty \mathrm{d}k\; D(k)\frac{\sin[(k^2-k_0^2)\tau/4]}{(k^2-k_0^2)/2} \times \exp[i(k^2-k_0^2)\tau/4 - ik^2t/2]e^{ikx} \tag{14}$$

for $t \geq \tau$. Here we have referred Eq. (13) for the definition of k_0. Note that $c(k,t)$ remains unchanged for $t > \tau$, but the wave packet still gains a free evolution phase $\exp(-ik^2t/2)$ after the pulse is over.

If the range of accessible continuum states is narrow, then the dipole matrix element $D(k)$ may be regarded as a constant within the range and moved out of the integral, replaced by value $D(k_0)$. This approximation is valid for relatively long pulses. For short few-cycle pulses, this approximation may break down, and an example will be given in the following subsection.

Then the shape of the photoelectron wave packet can be written as

$$\begin{aligned}\psi(x,t) &\approx -i\varepsilon_0 D(k_0)\int_0^\infty \mathrm{d}k \frac{\sin[(k^2-k_0^2)\tau/4]}{(k^2-k_0^2)/2} \times \exp[i(k^2-k_0^2)\tau/4 - ik^2t/2]e^{ikx} \\ &\equiv -i\varepsilon_0 D(k_0)\int_0^\infty \mathrm{d}k A(k) e^{i\phi(k,t)}e^{ikx},\end{aligned} \tag{15}$$

where we have defined

$$A(k) = \frac{\sin[(k^2-k_0^2)\tau/4]}{(k^2-k_0^2)/2}, \tag{16}$$

$$\begin{aligned}\phi(k,t) &= (k^2-k_0^2)\frac{\tau}{4} - \frac{k^2t}{2} \\ &= \frac{1}{2}\left(\frac{\tau}{2}-t\right)(k-k_0)^2 + \left(\frac{\tau}{2}-t\right)k_0(k-k_0) - \frac{t}{2}k_0^2.\end{aligned} \tag{17}$$

$A(k)e^{i\phi(k,t)}$ gives the weight of each plane wave component. We see that the function $\phi(k,t)$ contains a quadratic term centered on k_0, which is responsible for the shape of the photoelectron wave packet; a linear term, which is responsible for the spatial translation of the wave packet; and a constant term, which does not have a physical effect.

Figure 3 shows the function $A(k)$, *the quadratic component of* $\phi(k,t)$, and the resulting shape of the photoelectron wave packet for six different times to be compared to the middle column of Fig. 2. One sees very good qualitative agreements with the wave packet shapes obtained using the full dimensional TDSE, for all six times. The wave packet starts from a complex multipeak structure and then adjusts itself by reducing the number of peaks, eventually becoming a relatively simple single-peak structure.

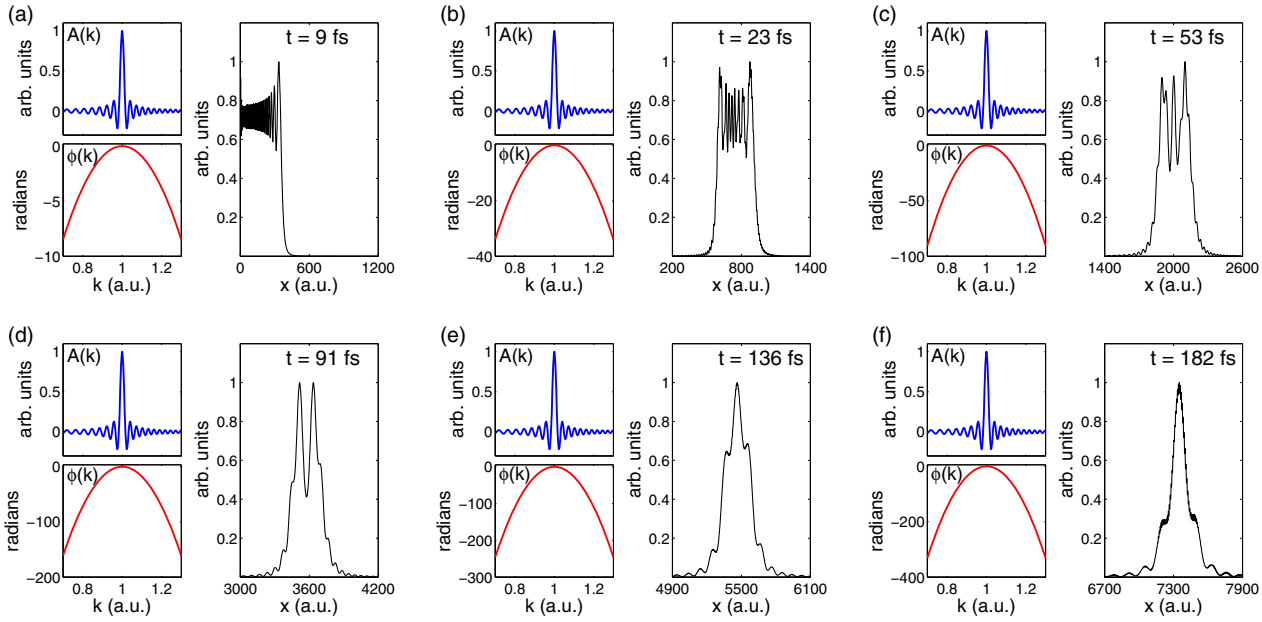

Fig. 3. Function $A(k)$, the quadratic component of the function $\phi(k,t)$, and the resulting shapes of the photoelectron wave packet predicted by Eq. (15). Notice the vertical scale of $\phi(k)$ for each panel. The shapes of the wave packets are to be compared to the middle column of Fig. 2.

C. Time Scale Estimations and Possible Experimental Tests

In this subsection we give estimations on the time scales involved and possible experimental tests on the shape of the photoelectron wave packets.

Let us take a closer look at the amplitude function $A(k)$ and the phase function $\phi(k,t)$ shown in Eqs. (16) and (17). Since only the quadratic phase term is responsible for the shape of the photoelectron wave packet, we write it separately as

$$\phi^{(2)}(k,t) = \frac{1}{2}\left(\frac{\tau}{2} - t\right)(k-k_0)^2. \tag{18}$$

The width of $A(k)$ is determined by the pulse duration τ, whereas the width of the stationary-phase region of $\phi^{(2)}(k,t)$ is determined mainly by the free-evolution time t. Figure 4(a) shows $A(k)$ and $\cos[\phi^{(2)}(k,t)]$ for $t = 9$ fs, that is, right after the 9-fs pulse is over (corresponding to the middle column of Fig. 2). One sees that the width of the stationary-phase region is much wider than the width of $A(k)$ at the beginning of free evolution. Therefore many k components contribute at a given position x [Eq. (15)], leading to a complicated multiple-peak structure.

As time t increases, the photoelectron flies to the detector, and the width of the stationary-phase region decreases. Eventually this width is much narrower than the width of $A(k)$, which remains unchanged after the laser pulse is over. Figure 4(b) shows $A(k)$ and $\cos[\phi^{(2)}(k,t)]$ for $t = 9$ ps, 1000 times the pulse duration. Note the change of the range of the horizontal axis compared to panel (a). The stationary-phase region is now much narrower than the width of $A(k)$. At a given position x, there is virtually only one k component that contributes. Free evolution disentangles different k components in space.

The final single-peak structure should be measurable experimentally. The key point is that the temporal resolution of the detector should be smaller than the temporal duration of the photoelectron wave packet. Let us now estimate this temporal duration Δt. The width of the stationary-phase region, at the time of detection, is estimated to be $\Delta k \sim 1/\sqrt{t} \approx 1/\sqrt{L/k_0} = \sqrt{k_0/L}$, where L is the distance from the laser focus (where photoionization happens) to the detector and k_0 is the center velocity of the wave packet. [See Fig. 4(c) for an illustration.] The spatial width of the wave packet is $\Delta x \approx 1/\Delta k \sim \sqrt{L/k_0}$ and the temporal duration of the wave packet is $\Delta t \approx \Delta x/k_0 \sim \sqrt{L/k_0^3}$. L is on the order of 1 m or about 10^{10} a.u.. If $k_0 = 1$ a.u., then $\Delta t \sim 10^5$ a.u. or 1 ps. If $k_0 = 0.01$ a.u., then $\Delta t \sim 10^8$ a.u. or 1 ns.

Modern microchannel plate detectors have temporal resolutions on the order of 10–100 ps [40]. Therefore the shape of the photoelectron wave packet should be measurable, provided that proper experimental parameters are chosen. A larger detector distance L and a smaller k_0 value lead to a larger Δt that can be resolvable experimentally.

D. Photoionization in the Few-Cycle Limit

For very short laser pulses, e.g., pulses consisting of only a few cycles, the dipole transition matrix element may change appreciably within the spectra of the laser pulses. Then in Eq. (14) we cannot move $D(k)$ out of the integral by assigning its value to be $D(k_0)$. The consequence is that each plane wave component will be further weighted by $D(k)$, resulting in a shift in the photoelectron momentum distribution and a different asymptotic photoelectron velocity.

Figure 5 shows the momentum distribution of the photoelectron for three different laser pulse durations, namely, 3 fs (blue solid), 1.2 fs (magenta dash dotted), and 0.75 fs (green dotted). As the pulse duration decreases, the photoelectron momentum distribution has two changes. First, the width increases; second, the peak position shifts. In this example, the peak shifts to the slower side, that is, a red shift. This can be understood from the shape of the dipole transition matrix element, the amplitude of which is shown in the same panel as the red-dashed curve. $|D(k)|$ decreases across the spectrum of the laser pulse (peaked in the neighborhood of $k = 1$), so it

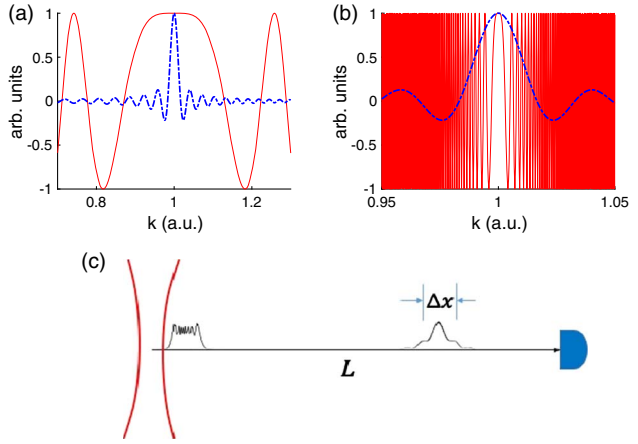

Fig. 4. (a) $A(k)$ (blue-dashed line) and $\cos[\phi^{(2)}(k,t)]$ (red solid line) for $t = \tau = 9$ fs, that is, right after the 9-fs laser pulse is over. (b) The same as (a), but for $t = 9$ ps. Note the different horizontal range from (a). (c) Illustration of the photoelectron wave packet flying from the laser focus to the detector. The distance is L. Δx is the spatial width of the wave packet.

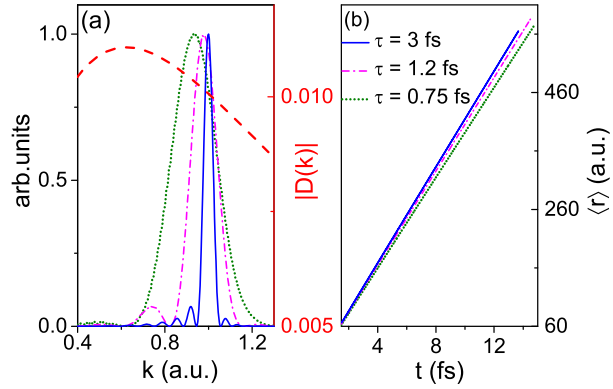

Fig. 5. (a) Photoelectron momentum distributions obtained with three laser pulse durations, namely, 3 fs (blue solid), 1.2 fs (magenta dash dotted), and 0.75 fs (green dotted). The red-dashed curve shows the shape of $|D(k)|$, the amplitude of the dipole transition matrix element (right vertical scale). (b) The corresponding time-dependent average position $\langle r\rangle(t)$ showing different asymptotic slopes.

effectively weights more the continuum states with smaller k values. The consequence is a red shift in the photoelectron momentum distribution as the pulse duration decreases.

In the time domain the photoelectron will have different asymptotic velocities, as shown in the right panel of Fig. 5. The time-dependent average position of the photoelectron $\langle r \rangle(t)$ has different asymptotic slopes for the three laser pulses.

Whether a few-cycle laser pulse leads to a slower or a faster asymptotic photoelectron velocity depends on the shape of the dipole transition matrix element $D(k)$. If the amplitude of $D(k)$ increases across the spectrum of the laser pulse, then it puts more weights on the faster components, and the asymptotic velocity of the photoelectron will be faster than that obtained with longer laser pulses.

4. CONCLUSION

In this paper we present a combined numerical and theoretical study of atomic photoionization in the time domain. Numerical results are obtained by solving the full dimensional time-dependent Schrödinger equation. And the numerical results are analyzed using the time-dependent perturbation theory. A time-domain study of the atomic photoionization process is motivated by rapid recent progress of ultrafast laser technology, which can generate laser pulses as short as a few tens of attoseconds.

We find that the shape of the photoelectron wave packet experiences rapid and dramatic changes after being emitted. Right after emission, the wave packet has a rather complex and multipeak structure, but it evolves rapidly with time by reducing the number of peaks. Eventually, the wave packet has a rather simple single-peak structure to be detected by a detector. This shape evolution process can be qualitatively explained by a simple model based on the time-dependent perturbation theory. The key factor is the quadratic component of the phase of the wave packet.

For long laser pulses, the spectra are usually narrow enough such that the dipole transition matrix element changes little within the spectra and can be treated as a constant. For short few-cycle laser pulses with relatively wide spectra, however, the dipole transition matrix element may change appreciably within the spectra of the laser. The consequence is a change in the photoelectron asymptotic velocity, either faster or slower, depending on the detailed form of the dipole transition matrix element.

Funding. National Natural Science Foundation of China (NSFC) (11774323); China Science Challenge Project (TZ2018005); NSAF Joint Fund (U1730449); National Key R&D Program (2017YFA0403200).

REFERENCES

1. H. Hertz, "Ueber einen einfluss des ultravioletten lichtes auf die electrische entladung," Ann. Phys. **267**, 983–1000 (1887).
2. P. Lenard, "Ueber die lichtelektrische wirkung," Ann. Phys. **313**, 149–198 (1902).
3. A. Einstein, "Über einen die erzeugung und verwandlung des lichtes betreffenden heuristischen gesichtspunkt," Ann. Phys. **322**, 132–148 (1905).
4. J. W. Cooper, "Photoionization from outer atomic subshells: a model study," Phys. Rev. **128**, 681–693 (1962).
5. U. Fano and J. W. Cooper, "Spectral distribution of atomic oscillator strengths," Rev. Mod. Phys. **40**, 441–507 (1968).
6. D. J. Kennedy and S. T. Manson, "Photoionization of the noble gases: cross sections and angular distributions," Phys. Rev. A **5**, 227–247 (1972).
7. F. Wuilleumier and M. O. Krause, "Photoionization of neon between 100 and 2000 eV: single and multiple processes, angular distributions, and subshell cross sections," Phys. Rev. A **10**, 242–258 (1974).
8. W. R. Johnson and C. D. Lin, "Multichannel relativistic random-phase approximation for the photoionization of atoms," Phys. Rev. A **20**, 964–977 (1979).
9. A. F. Starace, *Handbuch der Physik*, W. Mehlhorn, ed. (Springer, 1982), Vol. **XXXI**, pp. 1–121.
10. J. J. Yeh and I. Lindau, "Atomic subshell photoionization cross sections and asymmetry parameters: $1 \leq Z \geq 103$," At. Data Nucl. Data Tables **32**, 1–155 (1985).
11. U. Becker, D. Szostak, H. G. Kerkhoff, M. Kupsch, B. Langer, R. Wehlitz, A. Yagishita, and T. Hayaishi, "Subshell photoionization of Xe between 40 and 1000 eV," Phys. Rev. A **39**, 3902–3911 (1989).
12. M. Y. Amusia, *Atomic Photoeffect* (Plenum, 1990).
13. T. N. Chang, ed., *Many-Body Theory of Atomic Structure and Photoionization* (World Scientific, 1993).
14. U. Becker and D. A. Shirley, eds., *VUV and Soft X-Ray Photoionization Studies* (Plenum, 1996).
15. K. Zhao, Q. Zhang, M. Chini, Y. Wu, X. Wang, and Z. Chang, "Tailoring a 67 attosecond pulse through advantageous phase-mismatch," Opt. Lett. **37**, 3891–3893 (2012).
16. J. Li, X. Ren, Y. Yin, K. Zhao, A. Chew, Y. Cheng, E. Cunningham, Y. Wang, S. Hu, Y. Wu, M. Chini, and Z. Chang, "53-attosecond X-ray pulses reach the carbon K-edge," Nat. Commun. **8**, 186 (2017).
17. T. Gaumnitz, A. Jain, Y. Pertot, M. Huppert, I. Jordan, F. Ardana-Lamas, and H. Jakob Wörner, "Streaking of 43-attosecond soft-x-ray pulses generated by a passively CEP-stable mid-infrared driver," Opt. Express **25**, 27506–27518 (2017).
18. S. Huang, Y. Ding, Y. Feng, E. Hemsing, Z. Huang, J. Krzywinski, A. A. Lutman, A. Marinelli, T. J. Maxwell, and D. Zhu, "Generating single-spike hard x-ray pulses with nonlinear bunch compression in free-electron lasers," Phys. Rev. Lett. **119**, 154801 (2017).
19. G. Sansone, F. Kelkensberg, J. F. Pérez-Torres, F. Morales, M. F. Kling, W. Siu, O. Ghafur, P. Johnsson, M. Swoboda, E. Benedetti, F. Ferrari, F. Lépine, J. L. Sanz-Vicario, S. Zherebtsov, I. Znakovskaya, A. L'Huillier, M. Y. Ivanov, M. Nisoli, F. Martín, and M. J. J. Vrakking, "Electron localization following attosecond molecular photoionization," Nature **465**, 763–766 (2010).
20. M. Drescher, M. Hentschel, R. Kienberger, M. Uiberacker, V. Yakovlev, A. Scrinzi, T. Westerwalbesloh, U. Kleineberg, U. Heinzmann, and F. Krausz, "Time-resolved atomic inner-shell spectroscopy," Nature **419**, 803–807 (2002).
21. M. Uiberacker, T. Uphues, M. Schultze, A. J. Verhoef, V. Yakovlev, M. F. Kling, J. Rauschenberger, N. M. Kabachnik, H. Schröder, M. Lezius, K. L. Kompa, H.-G. Muller, M. J. J. Vrakking, S. Hendel, U. Kleineberg, U. Heinzmann, M. Drescher, and F. Krausz, "Attosecond real-time observation of electron tunnelling in atoms," Nature **446**, 627–632 (2007).
22. B. Erk, R. Boll, S. Trippel, D. Anielski, L. Foucar, B. Rudek, S. W. Epp, R. Coffee, S. Carron, S. Schorb, K. R. Ferguson, M. Swiggers, J. D. Bozek, M. Simon, T. Marchenko, J. Küpper, I. Schlichting, J. Ullrich, C. Bostedt, D. Rolles, and A. Rudenko, "Imaging charge transfer in iodomethane upon x-ray photoabsorption," Science **345**, 288–291 (2014).
23. A. Rudenko, L. Inhester, K. Hanasaki, X. Li, S. J. Robatjazi, B. Erk, R. Boll, K. Toyota, Y. Hao, O. Vendrell, C. Bomme, E. Savelyev, B. Rudek, L. Foucar, S. H. Southworth, C. S. Lehmann, B. Kraessig, T. Marchenko, M. Simon, K. Ueda, K. R. Ferguson, M. Bucher, T. Gorkhover, S. Carron, R. Alonso-Mori, J. E. Koglin, J. Correa, G. J. Williams, S. Boutet, L. Young, C. Bostedt, S.-K. Son, R. Santra, and D. Rolles, "Femtosecond response of polyatomic molecules to ultra-intense hard x-rays," Nature **546**, 129–132 (2017).
24. A. Kaldun, A. Blättermann, V. Stooß, S. Donsa, H. Wei, R. Pazourek, S. Nagele, C. Ott, C. D. Lin, J. Burgdörfer, and T. Pfeifer, "Observing

the ultrafast buildup of a Fano resonance in the time domain," Science **354**, 738–741 (2016).
25. M. Schultze, M. Fieß, N. Karpowicz, J. Gagnon, M. Korbman, M. Hofstetter, S. Neppl, A. L. Cavalieri, Y. Komninos, T. Mercouris, C. A. Nicolaides, R. Pazourek, S. Nagele, J. Feist, J. Burgdörfer, A. M. Azzeer, R. Ernstorfer, R. Kienberger, U. Kleineberg, E. Goulielmakis, F. Krausz, and V. S. Yakovlev, "Delay in photoemission," Science **328**, 1658–1662 (2010).
26. R. Pazourek, S. Nagele, and J. Burgdörfer, "Attosecond chronoscopy of photoemission," Rev. Mod. Phys. **87**, 765–802 (2015).
27. A. S. Kheifets and I. A. Ivanov, "Delay in atomic photoionization," Phys. Rev. Lett. **105**, 233002 (2010).
28. L. R. Moore, M. A. Lysaght, J. S. Parker, H. W. van der Hart, and K. T. Taylor, "Time delay between photoemission from the 2p and 2s subshells of neon," Phys. Rev. A **84**, 061404 (2011).
29. S. Nagele, R. Pazourek, J. Feist, and J. Burgdorfer, "Time shifts in photoemission from a fully correlated two-electron model system," Phys. Rev. A **85**, 033401 (2012).
30. J. M. Dahlström, T. Carette, and E. Lindroth, "Diagrammatic approach to attosecond delays in photoionization," Phys. Rev. A **86**, 061402 (2012).
31. J. M. Dahlström, A. L'Huillier, and A. Maquet, "Introduction to attosecond delays in photoionization," J. Phys. B **45**, 183001 (2012).
32. A. S. Kheifets, "Time delay in valence-shell photoionization of noble-gas atoms," Phys. Rev. A **87**, 063404 (2013).
33. J. Feist, O. Zatsarinny, S. Nagele, R. Pazourek, J. Burgdorfer, X. Guan, K. Bartschat, and B. I. Schneider, "Time delays for attosecond streaking in photoionization of neon," Phys. Rev. A **89**, 033417 (2014).
34. A. Maquet, J. Caillat, and R. Taïeb, "Attosecond delays in photoionization: time and quantum mechanics," J. Phys. B **47**, 204004 (2014).
35. H. Wei, T. Morishita, and C. D. Lin, "Critical evaluation of attosecond time delays retrieved from photoelectron streaking measurements," Phys. Rev. A **93**, 053412 (2016).
36. X.-M. Tong and S.-I. Chu, "Theoretical study of multiple high-order harmonic generation by intense ultrashort pulsed laser fields: a new generalized pseudospectral time-dependent method," Chem. Phys. **217**, 119–130 (1997).
37. D. J. Griffiths, *Introduction to Quantum Mechanics*, 2nd ed. (Cambridge University, 2017).
38. P. Krekora, Q. Su, and R. Grobe, "Effects of relativity on the time-resolved tunneling of electron wave packets," Phys. Rev. A **63**, 032107 (2001).
39. P. Krekora, Q. Su, and R. Grobe, "Critique of the Wigner tunneling speed and a proposed alternative," Phys. Rev. A **64**, 022105 (2001).
40. J. L. Wiza, "Microchannel plate detectors," Nucl. Instrum. Methods **162**, 587–601 (1979).